https://doi.org/10.5194/egusphere-2024-4116
Preprint. Discussion started: 26 May 2025

Characterizing orographic clouds and precipitation in Qilian Mountains, northwestern China

Jing Ren[1], Xiaoyan Wang[1], Wenqian Mao[3], Lingbin Kong[2]*, Zhenping Shao[4], and Wenyu Zhang[2]
1 Department of Atmospheric and Oceanic Sciences/ Institute of Atmospheric Sciences, Fudan University, Shanghai 200433
2 School of Computer and Artificial Intelligence, School of the Geo-science and Technology, Zhengzhou University, Zhengzhou 450001
3 College of Resources and Environmental Sciences, Gansu Agricultural University, Lanzhou 730000
4 Weather Modification Center of Henan Province, Zhengzhou 450001
*Corresponding author(s). E-mail(s): konglb@zzu.edu.cn

Abstract

Orographic precipitation has a critical role in water resource and hydrologic cycle in many arid and semiarid regions of the world. The formation and characteristics for an orographic precipitation event on 16-17 August 2020 in Qilian Mountains of northwestern China are investigated based on observational data and high-resolution (up to 333 m) simulations of WRF model. The results show that the local mountain-valley wind circulation has a critical role in the formation of orographic clouds and precipitation, showing an obvious daily variation. In the afternoon, due to strong solar radiation heating, there is an obvious upslope wind on the sunny side of the mountain, and the windward slope of the mountain was blocked and lifted, and a strong terrain wave was excited, resulting in strong convective clouds and precipitation. In the evening, due to the strong long-wave radiation cooling effect of the mountains, the strong downslope wind generated converges and lifts at the valley bottom, which promotes the development of weak convective and stratiform clouds over the valley. In the early hours of the morning, the downslope wind reaches its strongest level, producing a strong downhill wind circulation (mountain wind), and the downslope wind produces a strong uplift effect at the bottom of the valley, forming a deep layered cloud and precipitation process. In the afternoon, the convective clouds are dominant. The microphysical process is mainly characterized by high content of graupel particles. The sources of rainwater are mainly from the warm rain process and the melting process of graupel particles, accounting for 30.3% and 23.6% respectively. In the evening and early morning, the weak convective clouds and stratiform clouds are dominant. The melting of snow is the main source of rainwater, accounting for 92.6%; The precipitation conversion rate is basically consistent with the change trend of precipitation over time, and with the increase of terrain height, the precipitation conversion rate in this area also increases.

Keywords: Orographic Clouds and Precipitation, mountain-valley Wind Circulation, Microphysical properties, Qilian Mountains, northeastern Tibet Plateau

1 Introduction

Orographic clouds refer to clouds that are produced by the terrain forced uplift of airflow (Zhang et al., 2013; Guo et al., 2017), which is the main precipitation system

https://doi.org/10.5194/egusphere-2024-4116
Preprint. Discussion started: 26 May 2025

in the arid and semi-arid regions of northwestern China, and is also the main target clouds for artificial rainfall enhancement (Yi et al, 2019; Cheng et al., 2021; Qi et al., 2022）.

Leopold (1949) was a pioneer to study orographic clouds and proposed that the high topography of the Hawaiian Islands has a blocking effect on the trade wind, and the land-sea and valley circulation driven by surface thermal forcing produces standing wave cloud belts in the atmosphere. Andrea et al. (1997) simulated the effects of terrain factors and wet processes, and found that terrain plays a decisive role in the magnitude and distribution of rainfall, and sensible heat and latent heat processes only strengthen convective precipitation. The orographic cloud research program "Mesoscale Alps Project, MAP" has further improved the understanding of the formation process of orographic clouds when the air flow is blocked by mountains. Observational experiments with orographic clouds at high stability and low wind speeds have shown that a blockage develops at the lower level, leading to uplift and convection in the far southern regions of the mountain topography (Rotunno et al., 2003). Woods et al. (2005) analyzed a strong orographic precipitation process in the Cascade Mountains of Oregon, and concluded that the interaction between the front and the terrain enhances the precipitation, and the cloud can develop to a height of 8-9 km. Kirshbaum et al. (2007) concluded through observations and numerical simulations in Oregon that after airflow passes through small-scale obstacles, orographic lee waves will form updrafts at the leading edge of orographic clouds, which will trigger the formation of lee slope rainbands.

In the 1980s, the project of “Artificial Precipitation Experimental Research on Northern Stratiform Cloud” was carried out in Tianshan Mountains of Xinjiang, northwestern China. Tang et al. (2019) used WRF mode to conduct a numerical simulation study on cloud and precipitation under the influence of topography in the Naqu area of the Qinghai-Tibet Plateau, and found that the formation of orographic clouds is closely related to the intense solar radiation heating during the day, and clouds and precipitation in summer show an obvious diurnal variation. Zhang et al. (2020) used WRF mode to study the transport of water vapor in the Liupan Mountains,

https://doi.org/10.5194/egusphere-2024-4116
Preprint. Discussion started: 26 May 2025

and found that the dynamic forcing caused by terrain lifting has an obvious impact on summer precipitation. Qi et al. (2022) used WRF mode to study the spatial and seasonal distributions precipitation and precipitation efficiency in Qilian Mountains in the northeastern Qinghai-Tibet Plateau and its formation mechanisms. They found that precipitation generally increases with the terrain elevation below 3000 meters and decreases above 3000 meters.

Qilian Mountains are located in the arid and semi-arid region in northwestern China, bordering the Qinghai-Tibet Plateau on the south and the Hexi Corridor on the north (Yang et al., 2017; Wang et al., 2019; Cheng et al., 2021). Due to the terrain lifting of Qilian Mountains, it is conducive to the development of orographic clouds, with a maximum annual precipitation of 800 mm, which is an important supply of water resources in Qilian Mountains (Li et al., 2019; Yin et al., 2020; Chen et al., 2020). The orographic clouds in Qilian Mountains were investigated by Shao et al. (2013) and Cheng et al. (2021) and found that the uplift of terrain can promote the development of clouds and precipitation, and ice microphysical processes were significantly enhanced. The formation of orographic clouds in Qilian Mountains has a close relationship with the synoptic condition, vertical wind speed, and the uplift of terrain(Guo et al., 2013; Zhu et al, 2015). Zhang et al. (2021) and Liu et al. (2016) analyzed the variation characteristics of orographic clouds in the Qilian Mountains, and found that the water vapor in the orographic clouds in the Qilian Mountains is mainly distributed in the range of 3500-6500 m. And the cumulonimbus cloud formed only by orographic wind, heat and turbulence has a shorter duration and less precipitation.

The terrain and airflow itself are relatively complex, coupled with the nonlinear forcing effect of terrain on airflow, the current understanding of the role of Qilian Mountains in the transformation of water vapor-cloud-precipitation is not comprehensive enough, and there are few studies on the microphysical structure of topographic clouds and precipitation. Under complex terrain conditions, the low-level wind field is greatly affected by the terrain and has a high degree of inhomogeneity, and the range that the observation data can represent is very limited. Numerical

https://doi.org/10.5194/egusphere-2024-4116
Preprint. Discussion started: 26 May 2025

models can better describe the processes of cloud system development and precipitation generation, and are widely used in the study of cloud precipitation processes. In order to comprehensively reveal the role of the plateau's complex terrain and local atmospheric circulation in the formation of clouds and precipitation, it is necessary to use high-resolution numerical simulations of resolvable cloud processes.

This paper intends to investigate the typical topographic cloud precipitation process over the Qilian Mountains using the observation data of the Second Qinghai-Tibet Plateau Scientific Expedition Project and the Northwest Regional Weather Modification Project, combined with the resolvable cloud numerical model with high-resolution terrain data simulating the typical topographic cloud precipitation process over the Qilian Mountains. Using aircraft detection, weather radar, station precipitation, and other data to test the simulation results, on the basis that the simulation results are close to the actual situation, discuss the formation and evolution characteristics of clouds and precipitation under the complex terrain of the Qilian Mountains, and reveal the local atmospheric circulation in the clouds under the complex terrain, and its role in the formation and evolution of precipitation.

2 Data and model setup

2.1 Data

The paper uses the aircraft cloud detection data obtained by the artificial weather modification project in Northwest China, the observation data of CINRAD/CD weather radar (36.60°N, 101.78°E) at Xining Station in Qinghai Province, and the hourly precipitation data measured by observation stations on different underlying surfaces. The aircraft is equipped with Cloud Imaging Probe(CIP), Precipitation Imaging Probe(PIP), Hotwire LWC, and precipitation particle probes, cloud condensation nucleus counters and Aircraft-Integrated Meteorological Measurement System(AIMMS-20) produced by Droplet Measurement Technologies Inc.(DMT) in the United States. The main parameters of each probe are shown in Table 1. In addition, it also includes the hourly precipitation data fused by China's surface automatic weather stations and CMORPH, and the FNL(Final Operational Global Analysis(FNL) data provided by the National Center for Environmental Prediction

https://doi.org/10.5194/egusphere-2024-4116
Preprint. Discussion started: 26 May 2025

(NECP)/National Center for Atmospheric Research (NCAR).

Table 1 Main parameters of cloud microphysical probes

Probe Name	The object of the measurement	The range of measurement	Resolution
CIP	Cloud droplet distribution, concentration, two-dimensional image	25~1550 μm	25 μm
PIP	Precipitation particle spectral distribution, concentration, two-dimensional image	100~6200 μm	100 μm
Hotwire_LWC	Liquid water content	0~3 g/m3	-
AIMMS-20	Temperature, air pressure, humidity, wind, latitude and longitude, altitude	-	-

2.2 Model setup

The numerical simulation adopts the mesoscale model WRFV4.3, and the simulation time is from 20:00 on August 15, 2020 to 08:00 on August 17, 2020 (Beijing time, the same below). The model domains and physical processes setup are shown in Table 2 and Figure 1.

Table 2 Model setup

	d01	d02	d03	d04
Grid spacing	9 km	3 km	1 km	333 m
Horizontal grid number	112×112	232×232	403×355	532×511
Vertical grid number	34	34	34	34
Mode top height	50 hPa	50 hpa	50 hpa	50 hpa
Cumulus parameterization scheme	Grell-Devenyi	Grell-Devenyi	-	-
Boundary layer scheme	BMJ	BMJ	BMJ	BMJ
Land surface process scheme	RUC	RUC	RUC	RUC
Long wave radiation scheme	RRTM	RRTM	RRTM	RRTM
Cloud microphysical scheme	Thompson	Thompson	Thompson	Thompson
Surface layer scheme	Eta	Eta	Eta	Eta
Short wave radiation scheme	Goddard	Goddard	Goddard	Goddard

https://doi.org/10.5194/egusphere-2024-4116
Preprint. Discussion started: 26 May 2025

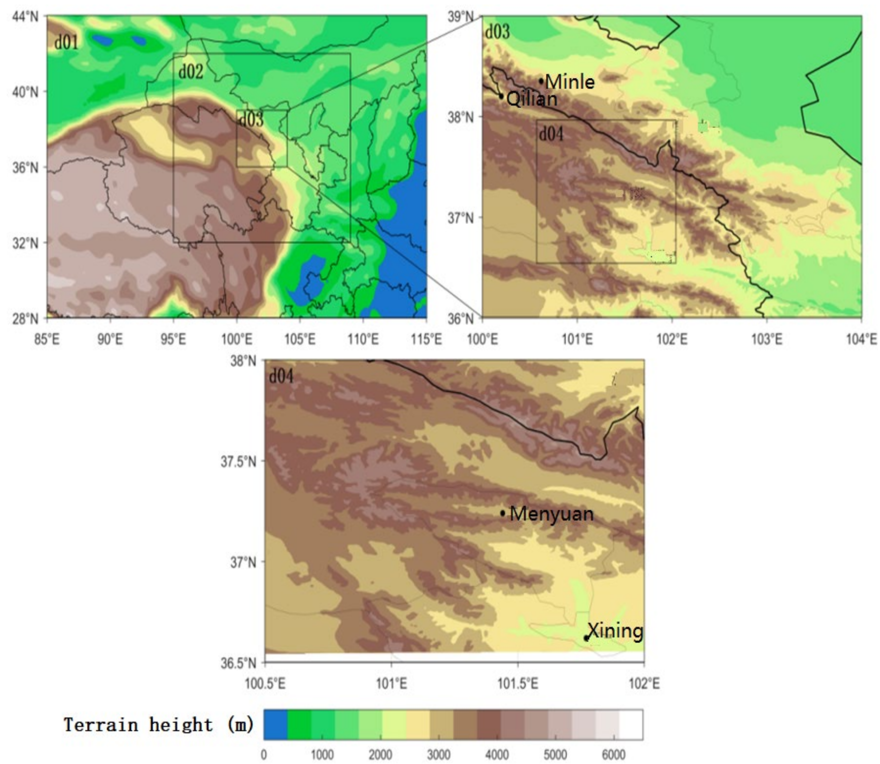

Figure 1 The model domain setup and terrain height (color shaded) in WRF model. d01 is the first domain, d02, the second nested domain, D03, the third nested domain range and D04 is the fourth nested domain.

3 Results

3.1 Synoptic conditions for the study case

From 16-17 August 2020, a precipitation cloud system appeared in the Xining area in the southeastern part of the Qilian Mountains from the early morning of the 16th to the early morning of the 17th. The spatial distribution of weather situation and water-vapor flux of 200 hPa, 500 hPa and 700 hPa at 10: 00 on 16 August 2020 are shown in Figure 2 and Figure 3. It can be seen that the northwest region is controlled by the high-altitude westerly trough, the temperature field in the trough lags behind the height field, there is strong cold air transport behind the trough, and warm air flows in front of the trough. The study area is located at the confluence of cold and warm airflow behind the front ridge of the high-altitude trough, controlled by the southwest airflow, and there are strong water vapor flux conveyor belts in the north

https://doi.org/10.5194/egusphere-2024-4116
Preprint. Discussion started: 26 May 2025

and southeast of it. Affected by the warm and humid southwest airflow and cold air in front of the trough, precipitation occurred in the study area. From the weather situation field at 700hPa, it can be seen that when the airflow meets the terrain, part of it flows around and part of it climbs up. The complex topography of the Qilian Mountains has an impact on the airflow.

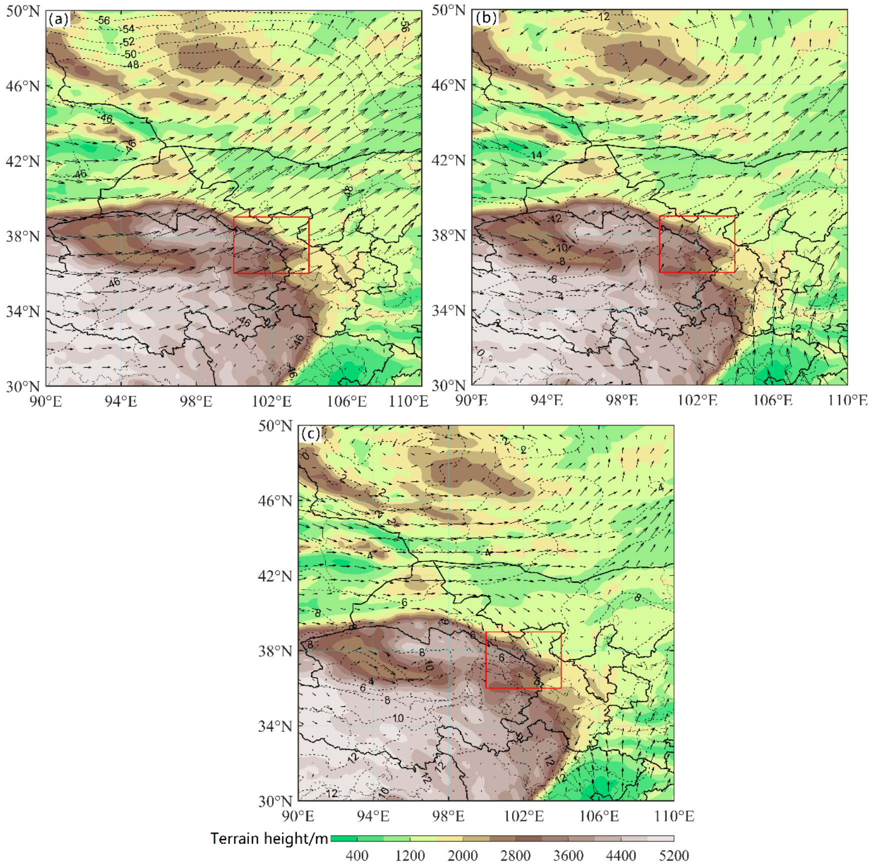

Figure 2 Spatial distribution of weather situation at 10:00 on August 16th, 2020.
（a）200hPa，（b）500hPa，（c）700hPa
(Height field, solid black line, unit: gpm； Temperature field, black dotted line, unit `1C; Wind field, black arrow; Red box, study area)

https://doi.org/10.5194/egusphere-2024-4116
Preprint. Discussion started: 26 May 2025

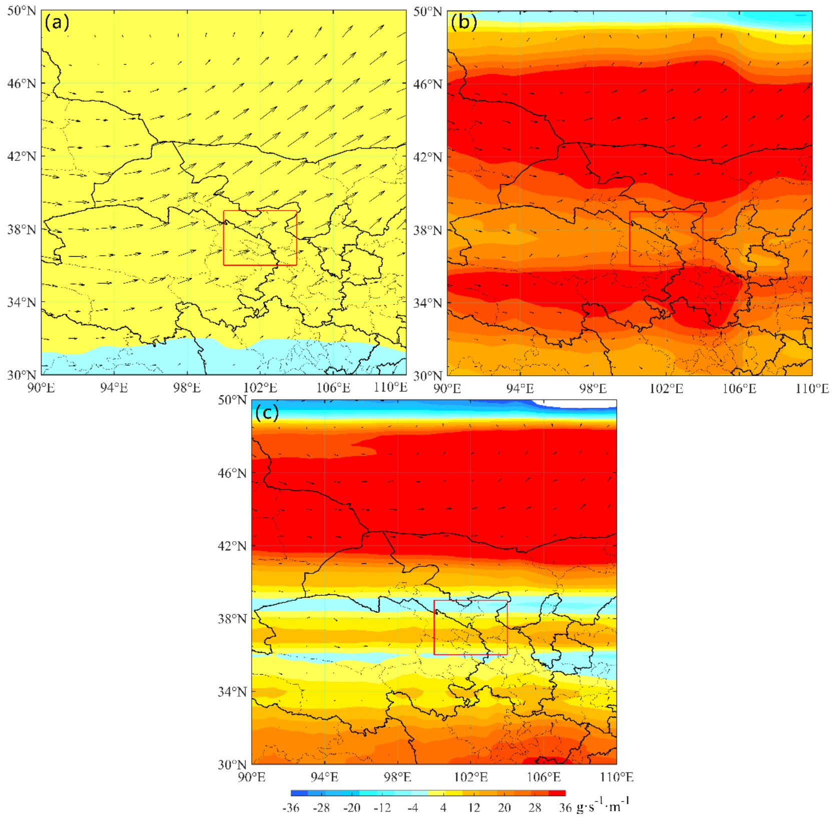

Figure 3 Spatial distribution of water-vapor flux at 10:00 on August 16th, 2020.

（a）200hPa，（b）500hPa，（c）700hPa

(Wind field, black arrow; Red box, study area)

The Black Body Temperature (TBB) observed by the Y-2G satellite is shown in Figure 4. The precipitation process on August 16, 2020 was mainly stratocumulus precipitation, the cloud layer developed deep and thick, and there was a strong updraft in some areas of the cloud area. The supercooled cloud body entered the research area on the morning of the 16th, and then the cloud system moved to the southeast. From the afternoon of the 16th, sporadic weak convective cells appeared in the study area, and then the convective cells developed and merged to form a large-scale cloud belt. By 18:00 on the 16th, the cloud top of the precipitation cloud was higher and the cloud layer was deep. In the early morning of the 17th, the cloud top temperature in most of the study area was lower than -40°C, and the intensity of the cloud system was weak (Figure 4a). It can be seen that the formation, development and weakening

https://doi.org/10.5194/egusphere-2024-4116
Preprint. Discussion started: 26 May 2025

of clouds have obvious diurnal variation characteristics.

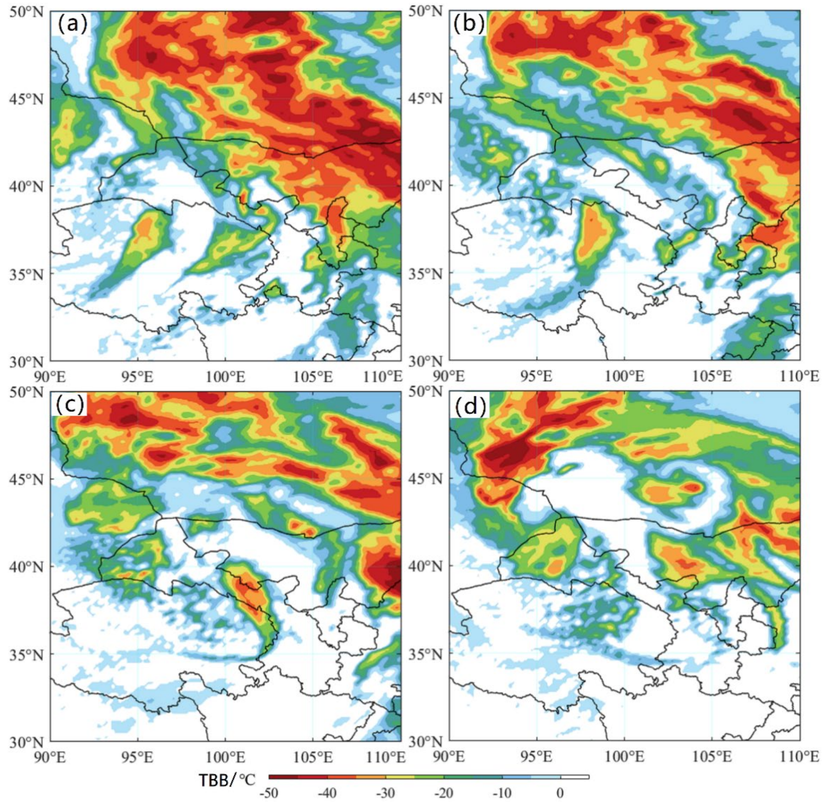

Figure 4 FY-2G satellite cloud image on August 16th, 2020 (the blue box is the research area).
(（a）10:00；（b）14:00；（c）19:00；（d）02:00)

3.2 Comparison of simulated clouds and precipitation against observations

Zhang et al. (2022) compared the combined reflectivity of radar echoes observed and simulated at 00:00, 09:00, and 19:00 on August 16, 2020. It is found that this precipitation process has typical stratocumulus precipitation echo characteristics, and columnar convective cloud echoes are inlaid in the relatively uniform echo layer. The edge of the echo is fragmented, and in a large range, it is the echo of stratiform cloud precipitation with an intensity less than 25 dBZ, but the echo of stratiform cloud is embedded with agglomerated strong echo, and the maximum value of the echo is 40 dBZ. At the same time, it is found that the precipitation system affecting the Qilian Mountains moves from southwest to northeast, and the simulated radar echoes also reflect this characteristic, and the positions of the simulated strong radar echoes are

https://doi.org/10.5194/egusphere-2024-4116
Preprint. Discussion started: 26 May 2025

also relatively close to the measured positions. The research by Zhang et al. showed that the WRF model simulated the precipitation process of the stratocumulus system in the Qilian Mountains more accurately, and with the elevation of the terrain, the observed and simulated radar echo changes were basically consistent.

The detection time of the aircraft data is from 08:50 to 12:00 on August 16, 2020. The detection cloud area is located near Menyuan County, Haibei Tibetan Autonomous Prefecture, Qinghai Province, at the eastern foot of Qilian Mountain. The three-dimensional trajectory of the aircraft flight is shown in Figure 5. The plane took off from Xining Airport at 08:54 and flew northeast. After flying over Menyuan County, Haibei Prefecture, Qinghai Province at 09:23, it continued to fly eastward to Qilian Mountain. From 09: 32 to 09:54, the plane was located over the ridge of Qilian Mountain, and it circled down from 6.9 km to 5.6 km, and then circled up from 5.6km to 7.8 km, with the detection heights of 6.9, 6.6, 6.2, 5.9 and 5.6 km. In this paper, the vertical detection process of 5.6-6.9 km and the simulation results of WRF model are selected for comparative analysis.

The comparison of the liquid water content detected by the aircraft in the 5.6-6.9 km area with height distribution and the simulated cloud water content is shown in Figure 6. The comparison between the distribution of the CIP particle number concentration detected by the aircraft in the area of 5.6-6.9 km with the height and the simulated ice crystal number concentration is shown in Figure 8. The vertical detection flight trajectory and radar echo distribution of the aircraft in the 5.6-6.9 km area, as well as the typical image of ice crystal particles are shown in Figure 8. It can be seen that when the aircraft detects vertically in the 5.6-6.9 km area, the LWC is unevenly distributed with height, and the variation range is 0-0.03 g m^{-3}. The cloud-water mixing ratio simulated by the model varies from 0 to 0.10 g/kg, which is slightly higher than the aircraft detection value. The maximum value of the cloud-water mixing ratio simulated by the model is 0.10 g/kg, at about 5.5 km, which is slightly lower than the maximum height of the observed LWC. The change of total particle concentration with height (Figure 7) shows that the change of total CIP particle concentration with height is similar to that of LWC. The total concentration of

CIP particles is the highest near 5.6 km and 5.9 km, close to 40L^{-1}, and above 6 km. In the cloud layer, the total concentration of CIP particles is reduced to between 0 and 10L^{-1}. The ice crystal number concentration simulated by the model is basically consistent with the observation at the maximum height, and reaches 600 L^{-1} at the highest point at about 5.9 km. The simulated ice crystal number concentration is generally higher than the observed CIP particle number concentration.

By comparing the LWC and CIP particle concentrations and particle spectra in Figure 6 and Figure 7, and the vertical distribution of the typical ice crystal image in Figure 8. It is found that the main growth mechanism of ice crystals at 5600 m (-5.1°C) is desublimation. At 6560 m (-9.9°C), a large number of aggregated ice crystals significantly broaden the particle spectrum, and the ice crystals mainly grow by sublimation and coalescence. At 7850 m (-17.6°C), a large number of ice crystal aggregates composed of radial dendritic ice crystals were observed, and coalescence growth is the main growth mode of ice crystals at this height. The above conclusions are consistent with the model simulation results. The simulation results show that the ice crystals mainly originate from the desublimation of ice crystals and are mainly consumed through automatic transformation into snow. Moreover, the rain mainly comes from the melting of snow and graupel, and the cold cloud process is dominant.

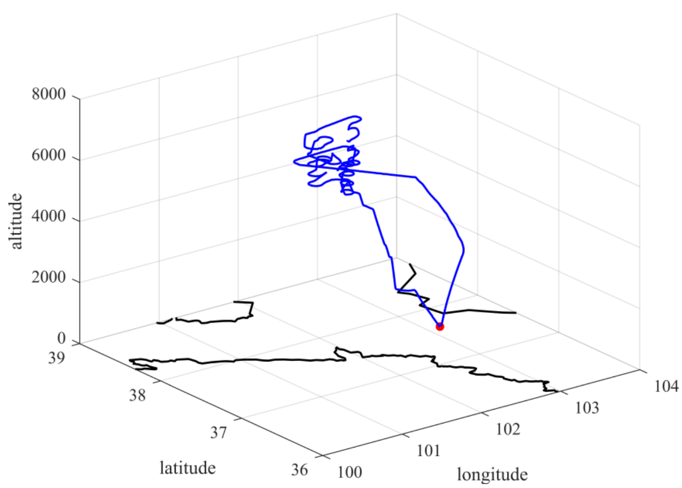

Figure 5 Three-dimensional trajectory of aircraft flight on August 16th, 2020.
(The blue line is a three-dimensional trajectory, the black line is the ground provincial boundary)

https://doi.org/10.5194/egusphere-2024-4116
Preprint. Discussion started: 26 May 2025

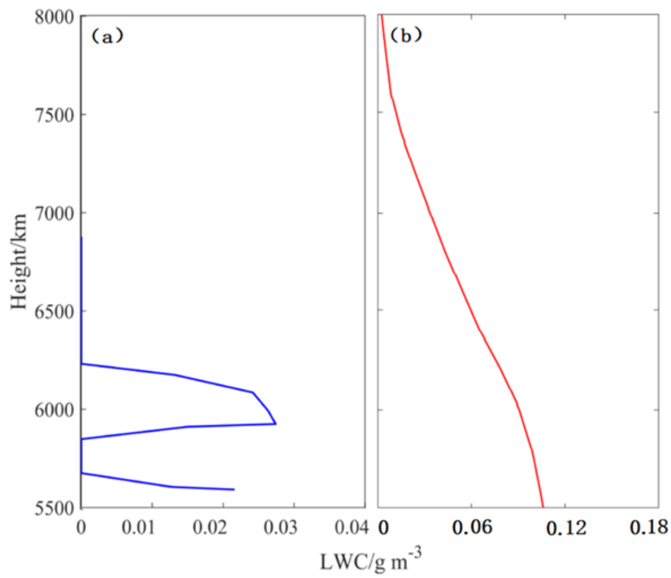

Figure 6 Comparison of liquid water content detected by aircraft with height distribution and simulated cloud water content at 5.6~6.9 km from 09: 32 to 09: 56 on August 16, 2020. （（a）liquid water content detected by aircraft; （b）simulated cloud water content）

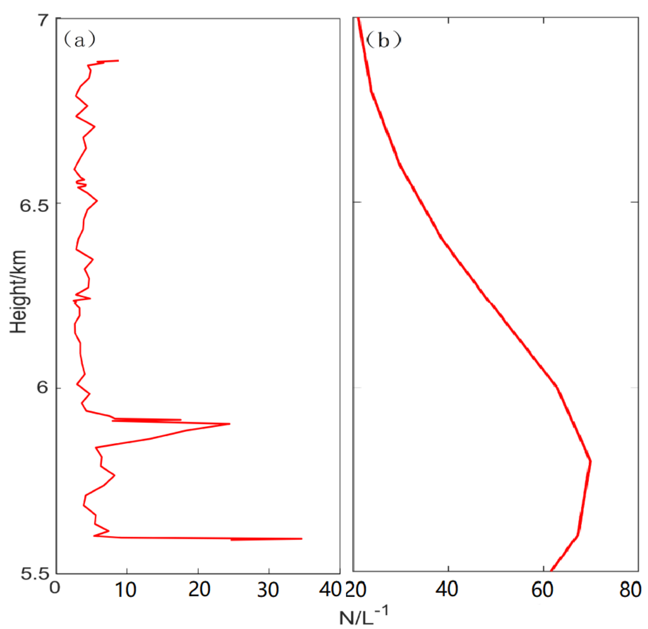

Figure 7 Comparison of CIP particle number concentration detected by aircraft with height distribution and simulated ice crystal number concentration in the area of 5.6~6.9 km from 09: 32 to 09: 56 on August 16th, 2020.（（a）CIP particle number concentration detected by aircraft,（b）simulated ice crystal number concentration）

https://doi.org/10.5194/egusphere-2024-4116
Preprint. Discussion started: 26 May 2025

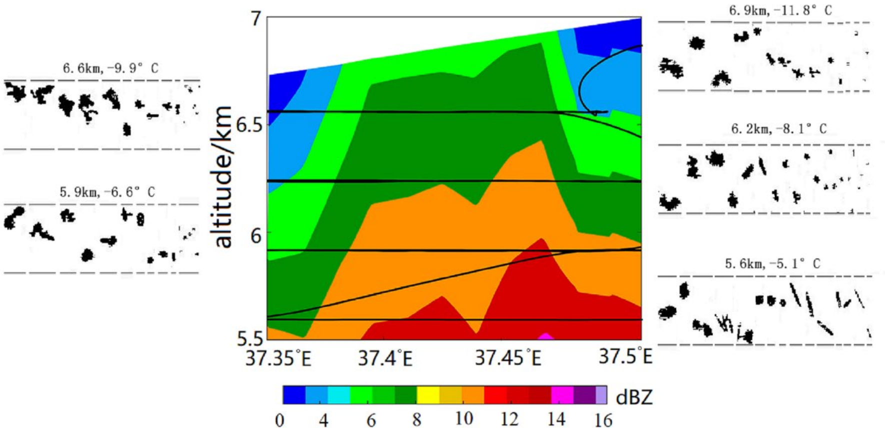

Figure 8 The flight trajectory (solid black line), radar echo distribution (color filling) and typical ice crystal particle images of the aircraft vertically detected at 5.6~6.9 km from 09: 32 to 09: 56 on August 16, 2020.

Figure 9 shows the spatial distribution of the 24h cumulative precipitation of the terrain in the d03 area on August 16, 2020, the numerical simulation of the Thompson scheme, station observations, and CMORPH data. Figure 9(a) shows the topography and distribution of stations in the d03 area, and Figure 9(b) shows the comparison between the observed precipitation at the d03 area station and the corresponding simulated values. The results show that the observed precipitation at the station is close to the simulated precipitation, and both the simulated and observed precipitation will increase as the terrain height increases. The climbing of the airflow, that is, the uplift of the terrain is an important factor affecting the precipitation in this cloud system. The spatial distribution of CMORPH's 24h cumulative precipitation is shown in Figure 9(c). It can be seen that the Thompson parameterization scheme can basically simulate the approximate location of the rain belt and the center of heavy precipitation, but the simulated rainfall and the range of the rain belt are somewhat larger than the actual measurement. The measured average value of the heavy precipitation center range is 25.32 mm, while the simulated heavy precipitation center range average value is 38.83 mm, which may be related to the error of the model itself, the influence of complex terrain in the study area, and the selected physical scheme.

https://doi.org/10.5194/egusphere-2024-4116
Preprint. Discussion started: 26 May 2025

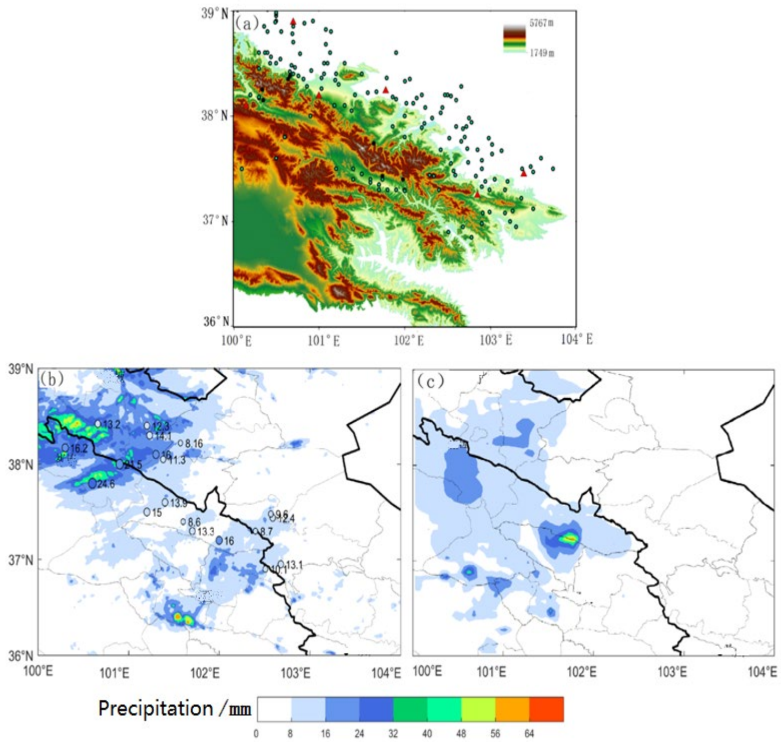

Figure 9 Comparison between the simulated and observed cumulative precipitation in d03 area on August 16th, 2020. (a) Distribution of rainfall stations and topography in the study area, (b) Colored dots denote the differences between simulations and measurements on 16 August 2020 in different stations. (c) Spatial Distribution of 24-hour cumulative precipitation of CMORPH data.

3.3 Characteristics of orographic clouds and precipitation in Qilian Mountains

The formation of orographic clouds and precipitation is often the result of multiple mechanisms, such as the uplift and blocking of the prevailing background airflow by terrain and the effect of orographic gravity waves (Guo et al., 2013). In addition, because terrains at different heights are heated by solar radiation and cooled by long-wave radiation, complex mountain-valley wind thermal circulation will be generated. The role and mechanism of this thermal circulation in the formation of orographic clouds and precipitation are still unclear. There is a southeast-northwest valley in the Xining area in the southeast of the Qilian Mountains, with peaks on both sides, and the maximum height difference between the mountains and the valley can reach more than 1500 m.

In order to reveal the characteristics of the mountain-valley wind circulation in the Xining area in the southeastern Qilian Mountains, the wind field is averaged for 24 hours (08:00 on August 16th to 08:00 on the 17th) to obtain the 24-hour average wind field, and then calculate the actual wind field the difference from the mean wind field (disturbed wind field). When the background circulation is relatively stable, the disturbance wind field can basically reflect the change of the wind field during the day and night. From the distribution of background atmospheric circulation shown in Figure 2, the background wind field in Xining area was relatively stable during August 16-17, so the change of disturbance wind speed can reflect the diurnal variation of valley wind circulation to a large extent Condition.

The distribution of average wind vectors in area d03 on August 16-17, 2020, and the horizontal distribution of disturbance wind vectors in area d04 in the afternoon, evening and early morning are shown in Figure 10. It can be seen that due to the influence of topography, the average wind in Xining is basically southeast, while the wind in its surrounding areas is basically northeast (Figure 10a). At 13:00 on August 16 (Figure 10b), due to the effect of solar radiation heating, the mountainous areas around Xining were basically upslope wind. While the upslope wind plays a dominant role, the southeast-northwest valley wind is obviously strengthened. At 19:00 in the evening of the same day (Figure 10c), due to the weakening of solar radiation, the surface long-wave radiation cooling process began to strengthen, resulting in the weakening of the upslope wind and the strengthening of the downslope wind. By 22:00, downhill winds were fully dominant. By 02:00 a.m. on August 17 (Figure 10d), due to the maximum long-wave radiative cooling, strong downslope and mountain wind outflows can be seen. In summary, even under the background of cloud and rainfall weather, the valley wind circulation in Xining area still has obvious diurnal variation characteristics, which shows that the valley wind circulation in Xining area is relatively strong due to the complex and high terrain. However, the role and impact of this diurnal variation in the formation of clouds and precipitation is still unknown.

https://doi.org/10.5194/egusphere-2024-4116
Preprint. Discussion started: 26 May 2025

The following is an analysis of the role and mechanism of wind circulation in valleys with complex terrain in the formation of clouds and precipitation according to the three stages previously divided.

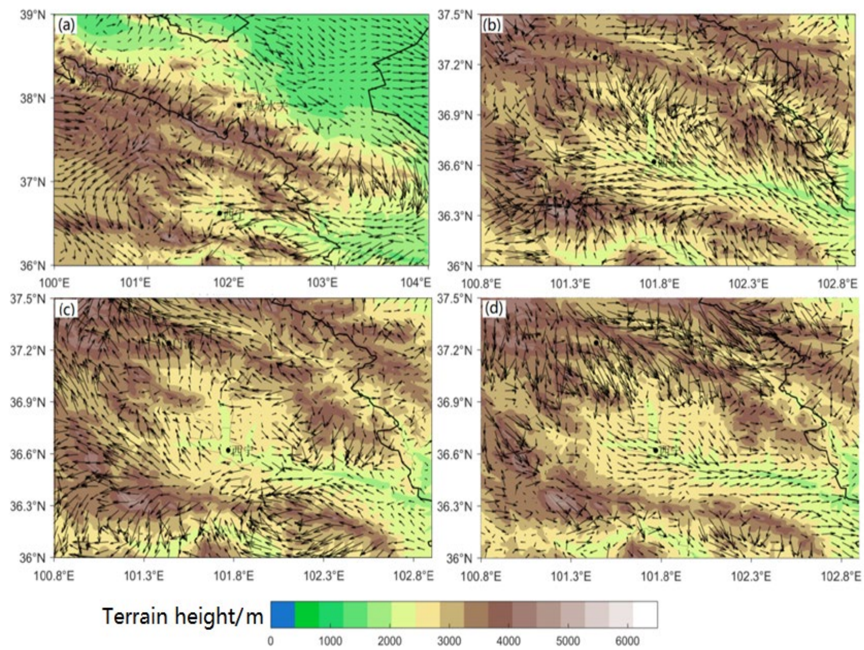

Figure 10 Average wind vector distribution in d03 area and disturbance wind vector in d04 area in the afternoon, evening and early morning on 16-17 August 2020.

The horizontal distribution of wind field and terrain height of 10 m on the ground at 13:00 on 16 August is shown in Figure 11(a). The cross-sectional distribution of AB line of vertical canyon in Figure 12a is shown in Figure 11(b). The cross-sectional distribution of CD line of vertical canyon in Figure 11a is shown in Figure 11(c). It can be seen that there is a strong upwelling wind at the valley bottom, and the sunny hillside is an uphill wind. This is because the sunny hillside is heated by solar radiation at a higher rate than the valley bottom, which leads to the decrease of air pressure on the sunny hillside and the top of the mountain, forming an air pressure gradient force from the valley to the top of the mountain, leading to the movement of air flow from the valley to the top of the mountain, thus forming an uphill wind. It can be seen that the formation of clouds and precipitation in the afternoon is mainly caused by the strong solar radiation heating on the hillside during the day, and the strong upper valley wind circulation is conducive to strengthening the warm and humid airflow flowing through the canyon. When the warm and humid airflow meets the uplift of the hillside, it forms a convective echo under the unstable atmospheric stratification condition. From the profile distribution of AB line and CD line of vertical canyon, it can be seen that the vertical airflow velocity (color filling) presents positive and negative alternating distribution, which is a typical distribution feature of topographic gravity waves (Guo Xin et al., 2013), which is caused by the propagation of topographic gravity waves caused by the collision between strong upper valley wind and terrain. It can be seen that the local circulation caused by plateau convection in the afternoon is complicated. In addition to the uplift of the upper valley wind flow by the hillside, the topographic gravity wave excited by the collision of the strong upper valley wind and the windward hillside also plays an important role, forming a deep convective precipitation process under the unstable atmospheric stratification conditions.

It can be seen that the formation of clouds and precipitation in the afternoon mainly occurs on the windward slope of the upper valley wind. Due to the strong solar radiation heating on the sunny hillside, the upper valley wind is strengthened after the formation of the uphill wind, and the strengthened upper valley wind is lifted after meeting with the windward slope, and the collision excites topographic gravity waves. In addition, the rapid heating of the sunny mountain range will also form a jet stream from the shady mountain range to the sunny side, which is beneficial to the further expansion and development of the clouds formed on the hillside. Under the condition of unstable atmospheric stratification, the main manifestation of clouds is convection.

The horizontal distribution of wind field and terrain height of 10 m on the ground at 19:00 on 16 August is shown in Figure 12(a). The cross-sectional distribution of AB line of vertical canyon in Figure 12a is shown in Figure 12(b). The cross-sectional distribution of CD line of vertical canyon in Figure 12a is shown in Figure 12(c). It can be seen that compared with the afternoon stage, the original upper valley wind is obviously weakened, and the reverse valley wind (lower valley wind) appears in some

https://doi.org/10.5194/egusphere-2024-4116
Preprint. Discussion started: 26 May 2025

canyons. Because the radiation cooling process of mountains plays a leading role, the downhill wind along the background prevailing wind side is more obvious, while the downhill wind against the background prevailing wind has a counteracting effect, and the downhill wind performance is not obvious. The convergence of downhill winds at the bottom of the valley has an obvious uplift effect, which promotes the development of clouds over the bottom of the valley, and the structure of clouds changes from afternoon convection to shallow convection and stratiform clouds.

The horizontal distribution of wind field and terrain height of 10 m on the ground at 02:00 on 17 August is shown in Figure 13(a). The cross-sectional distribution of AB line of vertical canyon in Figure 13a is shown in Figure 13(b). The cross-sectional distribution of CD line of vertical canyon in Figure 13a is shown in Figure 13(c). Figure 13a shows that the canyon area is basically downwind, and the downhill wind is dominant in the mountainous areas on both sides. A wide range of radar reflectivity has covered mountains and canyons. According to the vertical profile of AB (Figure 13b), the vertical structure of radar reflectivity mainly shows mixed clouds with a distribution height of 9 km, and the strong center is mainly distributed over the valley, which is related to the convergence and uplift of strong downhill wind at the valley bottom. Figure 13c shows that the northwest-southeast valley wind (mountain wind) in the lower level is obvious, and the cloud development over the canyon is relatively deep.

https://doi.org/10.5194/egusphere-2024-4116
Preprint. Discussion started: 26 May 2025

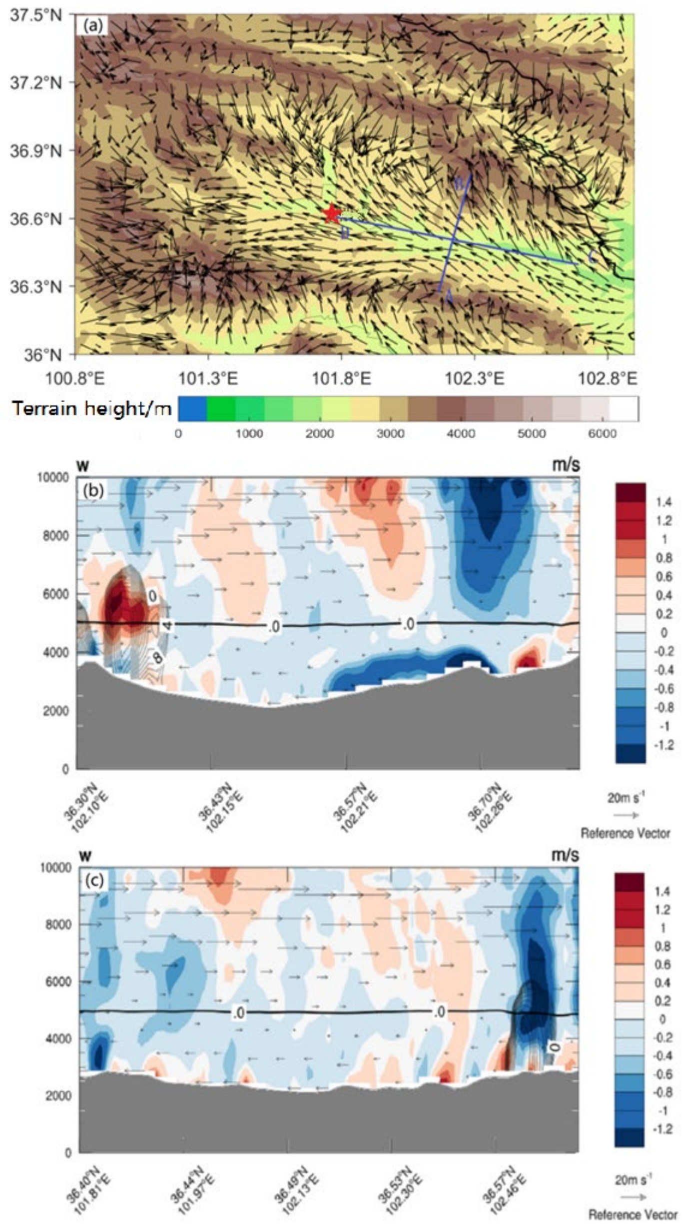

Figure 11 (a) horizontal distribution of perturbation wind vector at 10 m, and terrain height (color shaded) at 13:00 on 16 August 2020, (b) cross section of reflectivity (dBZ, solid lines), perturbation wind vector, vertical velocities (color shaded, m/s) and terrain (grey shaded) along AB line in Figure 11a, (c) same as in (b) but for that along CD line. Black solid line is the temperature of 0℃ at 13:00 on 16 August 2020. The red pentagram is the position of Xining station.

https://doi.org/10.5194/egusphere-2024-4116
Preprint. Discussion started: 26 May 2025

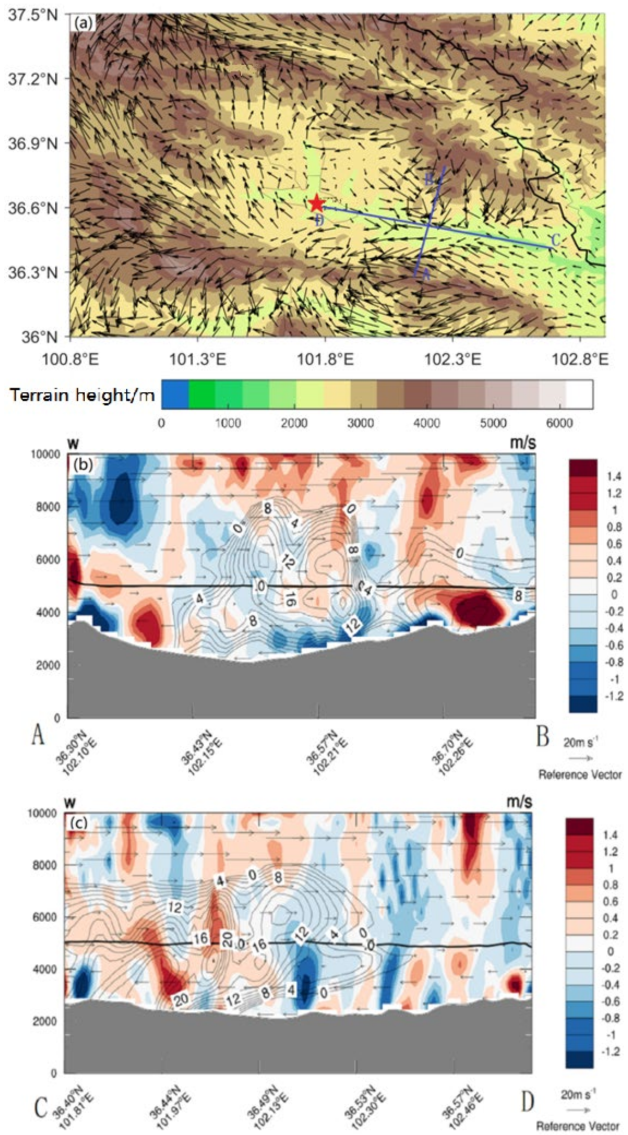

Figure 12: (a) horizontal distribution of perturbation wind vector at 10 m, and terrain height (color shaded) at 19:00 on 16 August 2020, (b) cross section of reflectivity (dBZ, solid lines), perturbation wind vector, vertical velocities (color shaded, m/s) and terrain (grey shaded) along AB line in Figure 12a, (c) same as in (b) but for that along CD line. Black solid line is the temperature of 0℃ at 19:00 on 16 August 2020. The red pentagram is the position of Xining station.

https://doi.org/10.5194/egusphere-2024-4116
Preprint. Discussion started: 26 May 2025

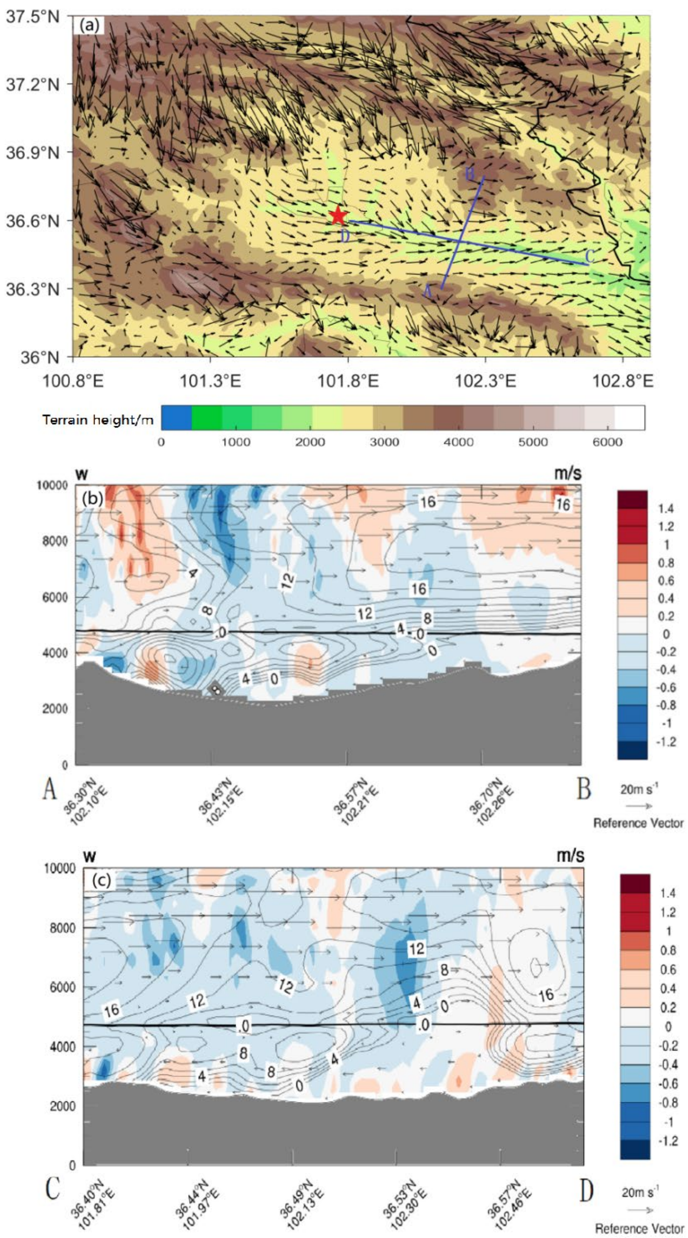

Figure 13 (a) horizontal distribution of perturbation wind vector at 10 m, and terrain height (color shaded) at 00:00 on 17 August 2020, (b) cross section of reflectivity (dBZ, solid lines), perturbation wind vector, vertical velocities (color shaded, m/s) and terrain (grey shaded) along AB line in Figure 13a, (c) same as in (b) but for that along CD line. Black solid line is the temperature of 0℃ at 00:00 on 17 August 2020. The red pentagram is the position of Xining station.

https://doi.org/10.5194/egusphere-2024-4116
Preprint. Discussion started: 26 May 2025

3.4 Properties of cloud microphysics and transformation processes

During the development of topographical clouds, topography plays a very important role. It not only affects the macroscopic structure and characteristics of clouds, but also largely affects the microphysical structure characteristics of precipitation development in clouds(Qi et al., 2019). The following is a quantitative analysis of cloud microphysical processes and transformation characteristics in different stages.

Figure 14 shows the evolution of the regional average values of the specific water content of the five types of water in the d03 region on 16 August 2020, including cloud water, rainwater, ice crystals, snow and graupel particles, over time. It can be seen that around 12:00 on 16 August, the content of supercooled cloud water reached 0.14g/kg, and the distribution height was between 4 km and 8 km. At this time, the local heat convection developed relatively vigorously. At the same time, it was found that the content of supercooled rainwater and graupel particles in the current stage is also relatively high, up to 0.12 g/kg and 0.2 g/kg respectively, but the content of snow is relatively small, and there are almost no ice crystals in the upper layer (or only the water content is lower than 0.01g/kg of trace ice crystals), indicating that the warm cloud process has a major contribution to the precipitation in the current stage. From the cloud microphysical height-time distribution from evening to early morning, cloud water, rain, and graupel content all weakened, but snow content increased significantly, indicating that the process of melting snow into rain increased significantly. It can be seen that the microphysical characteristics in the afternoon are mainly characterized by convective clouds, and the warm cloud process is dominant. From the evening to the early morning, it is mainly characterized by weak convection or stratiform clouds, indicating that the uplift of the terrain has promoted the enhancement of the microphysical processes of the ice phase, and the cold cloud process is dominant.

https://doi.org/10.5194/egusphere-2024-4116
Preprint. Discussion started: 26 May 2025

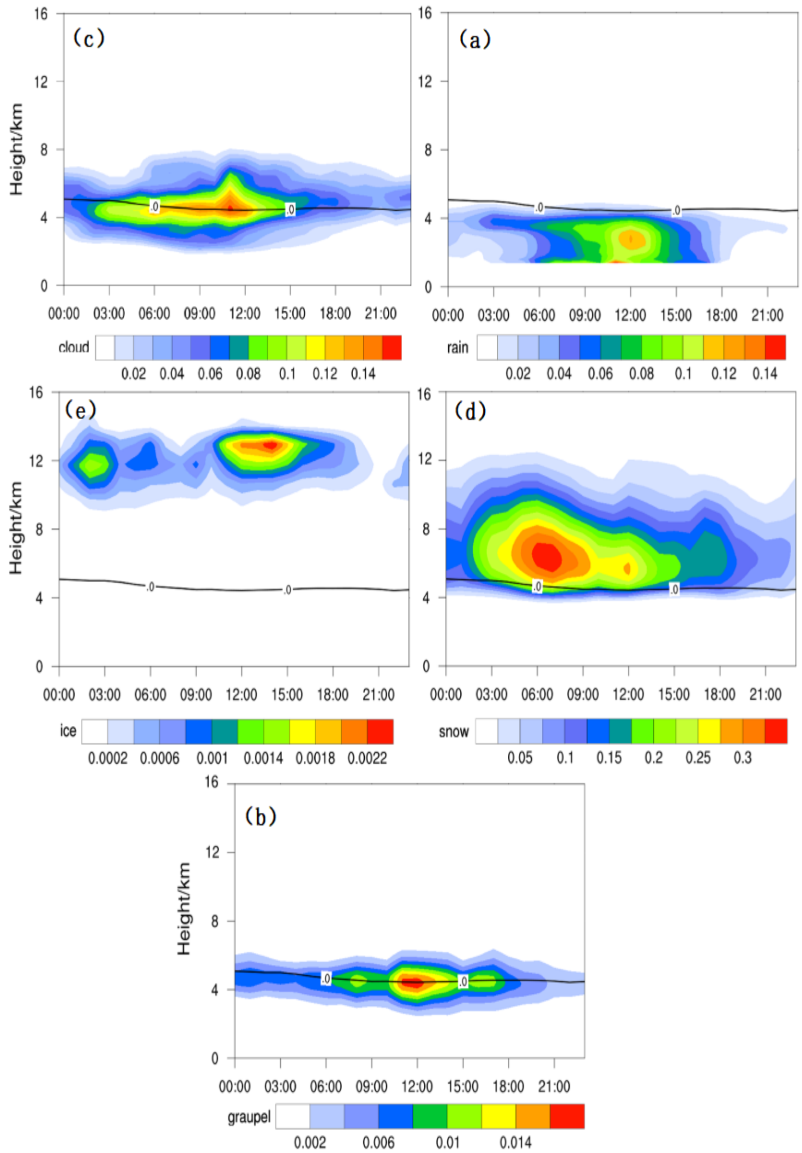

Figure 14 Evolution of regional average value of aquatic products with time height on 16 August 2020 (unit: g/kg, black isoline is 0 C line). (a) cloud water, (b) rain, (3) ice crystals, (d) snow and (e) graupel particles.

In order to further analyze the cloud microphysical transformation processes in different stages, the source and sink items of each hydrometeor are quantitatively analyzed.

https://doi.org/10.5194/egusphere-2024-4116
Preprint. Discussion started: 26 May 2025

Figure 15 shows the evolution of source and sink items of rainwater, cloud water, ice crystals, snow and graupel in d03 area with time, Figure 16 shows the vertical distribution profile of source and sink of aquatic products in d03 area, table 3 describes the main cloud microphysical processes, and tables 4 to 6 show the quantitative proportion of source and sink items of corresponding aquatic products in different stages. It can be seen that the growth of graupel particles in the afternoon thermal convection stage mainly depends on the collision and growth of graupel embryo with Leng Yun water (Prggcw), accounting for 34.5%. It includes the warm rain process in which 30.3% of rainwater meets and collects cloud water (Prrrcw), which plays a very important role in this stage, forming a large number of supercooled raindrops and providing the source of graupel embryo. In addition, the graupel particle melting process (Prrgml) at this stage is also an important source of rainwater, accounting for 23.6%. The role of snow particles in this stage is not obvious compared with 92.6% in other stages, but it still accounts for 35.6%. It is speculated that it may be the result of the high altitude and perennial snow in Qilian Mountain.

The process of cloud microphysical transformation is similar in the evening and early morning, and the transformation rate (Prgscw) of snow particles colliding with cloud and water is significantly increased, with the average proportion increasing from 39.6% to 85.6%. As a result, snow melting process (Prrsml) becomes the main source of rainwater, accounting for 92.6%, followed by the melting of graupel particles, accounting for 5.3%, and the warm rain process in which rainwater meets and collects cloud water, accounting for 0.9%. The proportion of graupel particles melting into rainwater decreased obviously, from 23.6% to 5.3%.

https://doi.org/10.5194/egusphere-2024-4116
Preprint. Discussion started: 26 May 2025

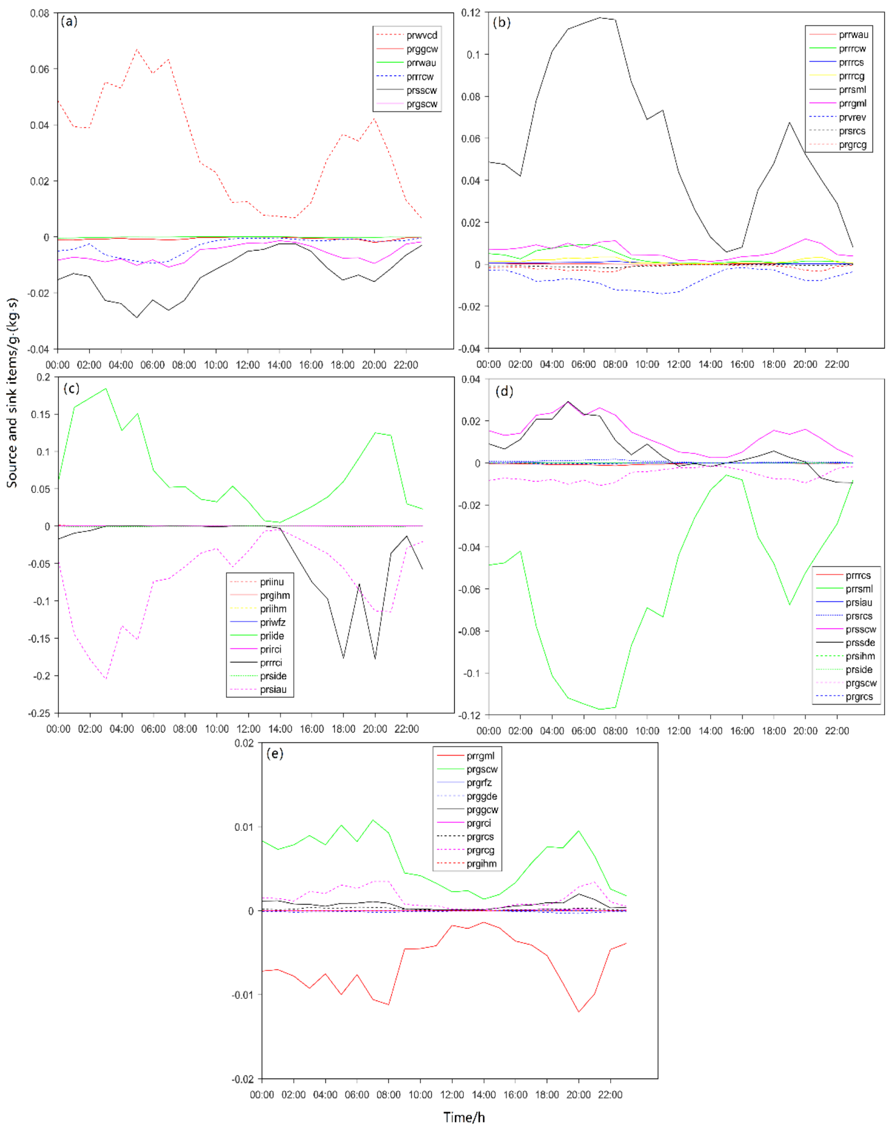

Figure 15 Variation of source and sink items of various aquatic products with time in d03 area on 16 August 2020 (unit 10-g/(kg s))
(a) cloud water, (b) rain water, (c) ice crystals, (d) snow, (e) graupel particles)

https://doi.org/10.5194/egusphere-2024-4116
Preprint. Discussion started: 26 May 2025

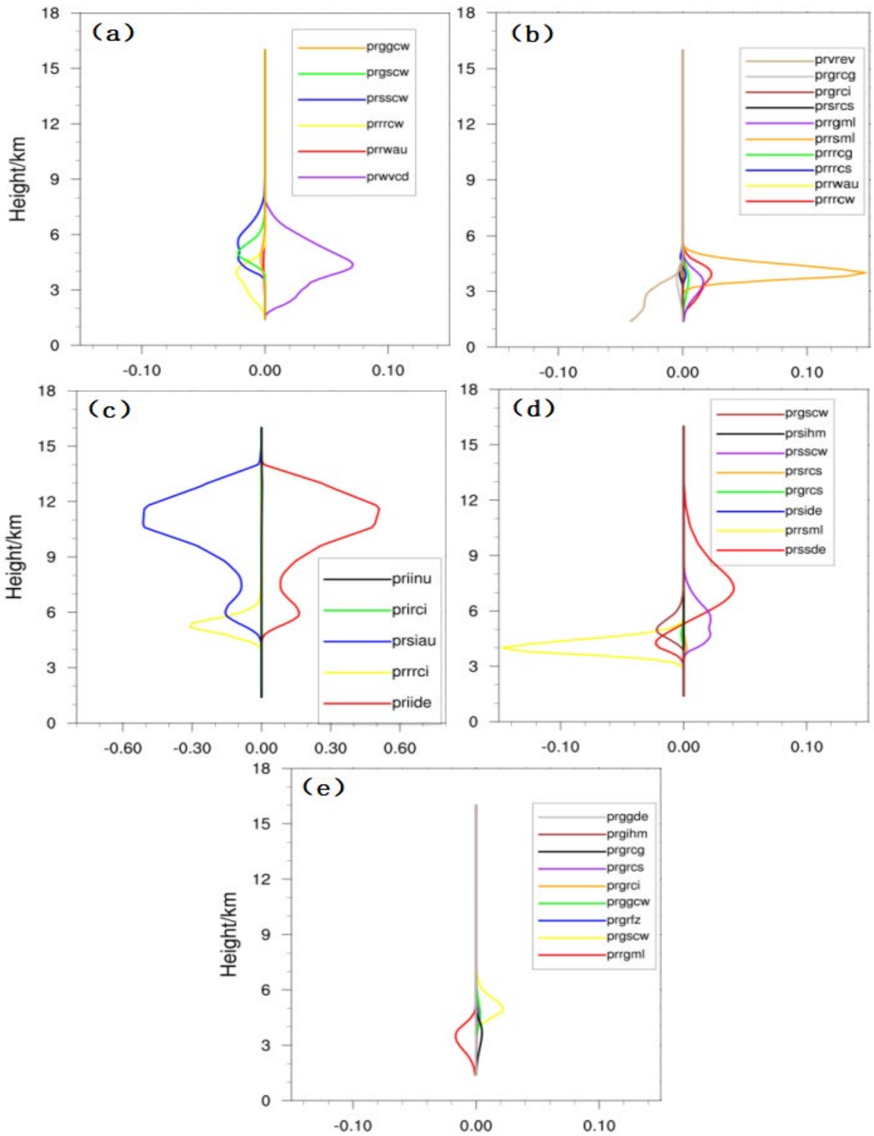

Figure 16 Vertical profile of source and sink items of aquatic products in d03 area on 16 August 2020. cloud water, (b) rain water, (c) ice crystals, (d) snow, (e) graupel particles)

4 Discussion

Compared with previous studies on the formation mechanism of terrain cloud precipitation, the role of valley wind circulation in the formation and evolution of

https://doi.org/10.5194/egusphere-2024-4116
Preprint. Discussion started: 26 May 2025

terrain clouds is more consistent, all of which have diurnal variation characteristics （Rotunno et al. (2003), Woods et al. (2005), Tang et al. (2019), Zhang et al.(2021), Qi et al. (2022)）. However, in the Qilian Mountains, due to its unique terrain and landforms, even under cloud and precipitation conditions, the complex and tall terrain still generates strong valley wind circulation, and shows more obvious diurnal variation characteristics.

Meanwhile, compared with previous studies on the microphysical structure characteristics of precipitation development within terrain clouds, with the uplift effect of terrain, the microphysical processes of ice phase will be enhanced, and the characteristics of microphysical structure will shift from warm cloud processes dominating to cold cloud processes dominating（Shao et al. (2013), Cheng et al. (2021), Guo et al. 2013, Zhu et al. (2015)）. However, there are certain differences in the specific changes in cloud microphysics in the Qilian Mountains compared to previous studies, and the reason for this difference may be due to its unique terrain and landforms.

5 Conclusions

This paper uses the observation data of weather radar, aircraft, station precipitation, etc. from the second scientific expedition to the Qinghai-Tibet Plateau and the artificial weather modification project in the northwest region combined with the WRF mesoscale numerical model. The role of valley wind circulation in the orographic cloud precipitation process during 16-17 August 2020 in the Xining region, southeast of the Qilian Mountains was studied, and the cloud microphysics and its transformation process were quantitatively studied.

（1） The precipitation process was caused by the passage of the westerly trough, and was affected by the warm and humid southwest airflow and cold air in front of the trough, resulting in precipitation in the study area. Through the comparison of station precipitation, weather radar, aircraft detection and other data with the simulated results, it was found that the model can basically simulate the approximate location of the rain belt and the heavy precipitation center in the Qilian Mountains, and the observed and simulated radar echo changes are relatively consistent. The ice crystal

https://doi.org/10.5194/egusphere-2024-4116
Preprint. Discussion started: 26 May 2025

number concentration and liquid water content simulated by the model are basically consistent with the observation results at the maximum height.

(2) The aircraft detection and simulation results show that the ice crystals mainly come from the desublimation of ice crystals, and are mainly consumed through automatic conversion into snow. The rain mainly comes from the melting of snow and graupel, and the cold cloud process is dominant.

(3) The local valley wind circulation in the Qilian Mountains plays an important role in the formation and evolution of clouds and precipitation. In the afternoon, due to the strong solar radiation heating in the mountains, firstly, there is an obvious upslope wind on the sunny side of the mountains, and the wind in the uphill valley is strengthened, and the mountain slopes are blocked and lifted, and strong gravity waves are stimulated, resulting in strong convective clouds and precipitation. In the evening, due to the strong long-wave radiation cooling effect of the mountains, downslope winds are generated, and the downslope winds converge and lift at the bottom of the valley, which promotes the development of weak convection and stratiform clouds over the valley, and produces heavy precipitation. In the early morning, the downslope wind reaches its strongest, and the downhill wind (mountain wind) is strengthened, which produces a strong uplift effect at the bottom of the valley, resulting in deep stratiform cloud precipitation.

(4) The topography of the Qilian Mountains affects the microphysical structure characteristics of precipitation development in clouds. The microphysical characteristics in the afternoon are mainly characterized by convective clouds, and the warm cloud process is dominant. The microphysical process of convective clouds is mainly manifested by the high content of graupel particles. The source of rainwater is mainly the warm rain process of rainwater colliding with and collecting cloud water and the melting process of graupel particles, accounting for 30.3% and 23.6% respectively. From the evening to the early morning, it is mainly characterized by weak convection or stratiform clouds, indicating that the uplift of the terrain has promoted the enhancement of the microphysical

processes of the ice phase, and the cold cloud process is dominant. The microphysical structure of weak convective clouds and stratiform clouds in the evening and early morning is similar, mainly due to the high content of snow particles, and the melting of snow is the main source of rainwater, accounting for 92.6%;

Author contribution: LK, XW, and JR planned the campaign; WM, ZS, WZ and JR performed the measurements; JR, XW analyzed the data; JR wrote the manuscript draft; XW, WM, LK, and ZS reviewed and edited the manuscript.

Competing interests: The authors declare that they have no conflict of interest.

Funding: This research was funded by the Second Tibetan Plateau Scientific Expedition and Research (STEP) Program of the Chinese Academy of Sciences grant number 2019QZKK0104, and the Research fund for Weather modification ability construction project of Northwest China grant number ZQCR18208.

Open Research: The FNL(Final Operational Global Analysis(FNL) data provided by the National Center for Environmental Prediction (NECP)/National Center for Atmospheric Research (NCAR). The FNL data are available at https://rda.ucar.edu/datasets/ds083.2/.

References

Buzzi, A., N. Tartaglione, P. Malguzzi, 1998: Numerical simulations of the1994 Piedmont flood:Role of orography and moist processes[J]. *Mon Wea Rev*, **1998**: 2369-2383.

Chen, Z., N. V. Koronovskii, 2020: The Active Modern Faults of the Western Segment of the Qilian Mountains (North Tibet). Moscow University Geology Bulletin, 75:211-219, doi:10.3103/S0145875220030035.

Cheng, P., H. Luo, Y. Chang, et al., 2021: Aircraft Measurement of Microphysical Characteristics of a Topog Cloud Precipitation in Qilian Mountains. *Journal of Applied Meteorological Science*, **32**: 691-705. （In Chinese）

Gong, N. G., M. P. Sun, L. X. Yan, et al., 2017: Temporal and spatial characteristics of atmospheric water vapor and its relationship with precipitation in Qilian Mountains during 1979-2016. *Arid Land Geography*, **40**: 762-771. （In Chinese）

Guo, X., X. L. Guo, D. H. Fu, et al., 2013: Relationship between bell-shaped terrain dynamic forcing, mountain wave propagation, and orographic clouds and precipitation. *Chinese Journal of Atmospheric Sciences (in Chinese)*, **37**: 786-800. （In Chinese）

Guo X., X. L. Guo, D. H. Fu, et al., 2017: Effects of CCN concentration on orographic clouds an ferent Froude numbers. *Acta Meteorologica Sinica*, **75**: 314-317.（In Chinese）

Herzegh P H, Hobbs P V. 1980. The mesoscale and microscale structure and organization of clouds and precipitation in midlatitude cyclones. II:Warm-frontal clouds [J]. J. Atmos. Sci., 37: 597–611.

Herzegh P H, Hobbs P V. 1981. The mesoscale and microscale structure and organization of clouds and precipitation in midlatitude cyclones. IV:Vertical air motions and microphysical structures of prefrontal surge clouds and cold-frontal clouds [J]. J. Atmos. Sci., 38 (8): 1771–1784.

Hou T J, Lei H C, Hu Z X, et al. 2013. Observations and modeling of ice water content in a mixed-phase cloud system [J]. Atmos. Oceanic Sci.Lett., 6 (4): 210–215.

Hu Z X, Lei H C, Guo X L, et al. 2007. Studies of the structure of a stratiform cloud and the physical processes of precipitation formation [J]. Chinese Journal of Atmospheric Sciences (in Chinese), 31 (3): 425–439. （In Chinese）Kirshbaum, D. J., H. B. George, R. O. Richard, 2007: The triggering of orographic rainbands by smal-l scale topogra-phy. *J Atmos Sci*, **64**: 1530-1549.

Li, L., J. Li, H. Chen, et al. 2019: Diurnal variations of summer precipitation over the Qilian Mountains in Northwest China. Meteorol. Res, 2019: 18-30.

Li, X., X. H. Guo, N. L. Wang, et al., 2019: Tightening ecological management facilitates green development in the Qilian Mountains. *Chinese Science Bulletin-Chinese*, **64**:2928-2937. doi: 10.1360/TB-2019-0209.（In Chinese）

Leopold, L. B., 1949: The interaction of trade wind and sea breeze, Hawaii [J]. *Journal of Meteorology*, **6**: 312-320.

Liu, B., 2016: Diurnal Changes of Summer Orographic Clouds on Southern Slope of Qilian Mountains and Impacts of Mountain-Valley Breeze. *Meteorological Science and Technology*, **44**: 67-75. （In Chinese）

Liu, Y. B., L. G. You, Z. J. Hu, et al., 1988: A Study on the Frontal Snowfall in Zhungeer Basin of Xinjiang in Winter, Part I : Precipitation Pattern. *Journal of Applied Meteorological Science,* **1988**: 36-45.（In Chinese）

Lawson R P, Zuidema P. 2009. Aircraft microphysical and surface-based radar observations of summertime arctic clouds [J]. J. Atmos. Sci., 66 (12): 3505–3529.

Lang S E, Tao W K, Zeng X P, et al. 2011. Reducing the biases in simulated radar reflectivities from a bulk microphysics scheme: Tropical convective systems [J]. J. Atmos. Sci., 68 (10): 2306–2320.

Lu G X, Guo X L. 2012. Distribution and origin of aerosol and its transform relationship with CCN derived from the spring multi-aircraft measurements of Beijing Cloud Experiment

(BCE) [J]. Chin. Sci. Bull., 57 (19): 2460–2469.

Mei, Q., X. Z. Fei, J. Wang, 2018: Verification and consensus experiments of rainstorm forecasting using different cloud parameterization schemes in WRF model. Transactions of Atmospheric Sciences, 41: 731-742. （In Chinese）

Miao, C., Y. Q. Zhou, J. Z. Liu, et al., 2020: Quantifying the cloud water resource: Methods based on observational diagnosis and cloud model simulation. J. Meteor. Res., 34, 1256-1270.

Qi, P., X. L. Guo, Y. Chang, et al., 2022: Cloud water path, precipitation amount, and precipitation efficiency derived from multiple datasets on the Qilian Mountains, Northeastern Tibetan Plateau[J]. *Atmospheric Research,* **274**: 798-818.

Qi, P., X. L. Guo, G. X. Lu, et al., 2019: Aircraft Measurements of a Stable Stratiform Cloud with Embedded Convection in Eastern Taihang Mountain of North China: Characteristicsof Embedded Convection and Melting Layer Structure. *Chinese Journal of Atmospheric Sciences (in Chinese)*, **43**: 1365-1384. （In Chinese）

Ren, J.; Zhang, W.; Kou, M.;Ma, Y.; Zhang, X. A Numerical Study of Critical Variables on Artificial Cold Cloud Precipitation Enhancement in the Qilian Mountains, China. Atmosphere 2023, 14, 1086.https://doi.org/10.3390/atmos14071086.

Rotunno, R., R. Ferretti, 2003: Orographic effects on rainfall in MAP cases IOP 2b and IOP 8[J]. *J. Roy. Meteor. Soc.*, **129**: 373-390.

Shao, Y.T., Q. J. Liu, Z. J. Jin, et al., 2013: Numerical Simulation on Macrophysics and Microphysics Structure of the Orographic Cloud and Precipitation in Summer of the Qilian Mountains. Journal of Arid Meteorology, 31: 18-23. （In Chinese）

Thompson, G., R. M. Rasmussen, K. Manning. 2004. Explicit forecasts of winter precipitation using an improved bulk microphysics scheme. Part I: Description and sensitivity analysis [J]. *Monthly Weather Review*, **132**: 519-542. doi:10.1175/1520-0493(2004)1322.0.co;2.

Tang, J., X, L, Guo, Y, Chang, et al., 2019: A Numerical Investigation on Microphysical Properties of Clouds and Precipitation over the Tibetan Plateau in Summer 2014. *J. Meteor. Res,* **33**: 463-477.

Wang, Y. F., J. J. Wang, X. Z. Yin, et al., 2019: Cloud characteristic parameters and artificial precipitation in the Qilian Mountains: research progress and prospect. *Journal of Glaciology and Geocryology*, **41**: 434-443. （In Chinese）

Woods, C. P., T. S. Mark, D. L. John, et al., 2005: Microphysical processes and synergistic interaction between frontaland orographic forcing of precipitation during the 13 December 2001IMPROVE-2 event over the oregon cascades[J]. *J Atmos Sci-Special Section*, **62**: 3493-3519.

Yang, L. R., J. X. Li, L. P. Yue, H. L. Wang, et al., 2017: Paleogene-Neogene stratigraphic realm and tectonic-sedimentary evolution of the Qilian Mountains and their surrounding areas. *Science China Earth Sciences*, **60**: 992–1009, doi: 10.1007/s11430- 016-9030-2.

Yang M. J., 2019: Differences in Cloud Vertical Structures between the Tibetan Plateau and

Eastern China Plains during Rainy Season as Measured by CloudSat/CALIPSO. *Advances in Meteorology*, **2019**: 1201-1212. doi: 10.1155/2019/6292930.

Yin, X. Z., Y. R. Wang, W. J. Xu, et al., 2020: Recent Progress in Research on Potential for the Development of Cloud Water Resources over Qilian Mountains Area. *Desert and Oasis Meteorology,* **14**: 134-140.（In Chinese）

Zhang, W. Y., Y. Huang, X. Z. Yin, et al., 2021: Observations and Research Progress of Cloud-Seeding (Snow) Project in Qilian Mountains. *Advances in Meteorological Science and Technology,* **11**: 102-116. （In Chinese）

Zhang, Y., R. C. Yu, J. Li, et al., 2013: Dynamic and Thermodynamic Relations of Distinctive Stratus Clouds on the Lee Side of the Tibetan Plateau in the Cold Season. *Journal of Climate*, **26**: 8378-8391. doi: 10.1175/JCLI-D-13-00009.1. Zhang, P., Z. Y. Yao, S. Jia, et al., 2020: Study of the Characteristics of Atmospheric Water Resources and Hydrometeor Precipitation Efficiency over the Liupan ShanArea. *Chinese Journal of Atmospheric Sciences (in Chinese)*, **44:** 421-434. doi:10.3878/j.issn.1006-9895.1904.19104. （In Chinese）

Zhu, P., G. Q. Zhang, 2015: Radar Echo Characteristics of Orographic Cloud in Huangshui River-vale, South of Qilian Mountain. *Arid Zone Research,* **32**: 551-564. （In Chinese）

Zhu S C, Guo X L. 2014. Ice crystal habits, distribution and growth process in stratiform clouds with embedded convection in North China: Aircraft measurements [J]. Acta Meteorologica Sinica (in Chinese), 72 (2): 366–389.